**D. C. GAKENHEIMER**[2]
Mem. ASME

**J. MIKLOWITZ**
Professor of Applied Mechanics.
Mem. ASME

California Institute of Technology,
Pasadena, Calif.

# Transient Excitation of an Elastic Half Space by a Point Load Traveling on the Surface[1]

*The propagation of transient waves in a homogeneous, isotropic, linearly elastic half space excited by a traveling normal point load is investigated. The load is suddenly applied and then it moves rectilinearly at a constant speed along the free surface. The displacements are derived for the interior of the half space and for all load speeds. Wave-front expansions are obtained from the exact solution, in addition to results pertaining to the steady-state displacement field. The limit case of zero load speed is considered, yielding new results for Lamb's point load problem.*

## 1 Introduction

Ground motions excited by moving surface forces arise, for example, from nuclear blasts and from shock waves generated by supersonic aircraft, and they interact with structures causing extensive damage. A mathematical problem of fundamental importance in these applications is that of an elastic half space whose surface is excited by a normal point load which is suddenly applied and which subsequently moves rectilinearly at a constant speed.

In recent years several solutions to this problem have been given for the surface of the half space. First, Payton [1][3] computed the transient surface displacements by using an elastodynamic reciprocal theorem. Then Lansing [2] rederived some of Payton's results by employing a Duhamel superposition integral. However, no transient solutions have been given for the interior of the half space, which are of interest with regard to buried structures. Therefore, it was appropriate to seek the interior displacements here. The remaining contributions to this problem are the steady-state results given by Mandel and Avramesco [3], Papadopoulos [4, 5], Grimes [6], Eason [7], and Lansing [2].

Of further interest is the fact that a point load moving on the surface of a half space generates a nonaxisymmetric disturbance. Very few wave-propagation problems of this type have been solved and, in particular, no transient solutions have been derived for the interior of the half space. Chao [8] has analyzed the disturbance due to a tangential surface point load. However, like the moving load cases just mentioned, he only obtained a transient solution for the surface of the half space. Papadopoulos [4] has considered the nonaxisymmetric problems of a buried tangential point load and a couple force, but he also only gave detailed transient results for the surface. Further, Scott and Miklowitz [9] have derived transient solutions for nonaxisymmetric plate problems, but their work has not been extended to half spaces. On the other hand, transient solutions are derived here for the interior of the half space and the solution technique is sufficiently general that it should contribute guidelines for analyzing other nonaxisymmetric half space problems.

After formulating the problem in section 2, a formal solution is obtained in section 3 by using the Laplace and double Fourier transforms. Then in section 4 the inverse transforms are evaluated by a technique due originally to Cagniard [10], but simplified by a transformation introduced by deHoop [11] for problems in acoustics and later used by Mitra [12] for an elastic half-space problem. In this way each displacement for the interior of the half space is reduced to a sum of single integrals and algebraic terms for all values of the load speed. Each contribution to the displacements is identified as a specific wave. In particular, the integrals represent waves which emanate from the initial position of the load as if they were generated by a stationary point source, while the algebraic terms represent disturbances that trail behind the load and whose wave geometry depends on the speed of the load relative to the body wave speeds. In section 5 this form of the solution is exploited to evaluate the displacements near the wave fronts. Then in section 6 the limit case of zero load speed is considered, showing that the integrals become a solution of Lamb's point load problem. Finally, in section 7, the algebraic terms are shown to form the steady-state displacement field when the load speed exceeds both the body wave speeds.

[1] This work was sponsored by the National Aeronautics and Space Administration and the Office of Naval Research.

[2] Now at RAND Corporation, Santa Monica, Calif.

[3] Numbers in brackets designate References at end of paper.

Contributed by the Applied Mechanics Division and presented at the Applied Mechanics Western Conference, Albuquerque, N. Mex., August 25–27, 1969, of The American Society of Mechanical Engineers.

Discussion of this paper should be addressed to the Editorial Department, ASME, United Engineering Center, 345 East 47th Street, New York, N. Y. 10017, and will be accepted until October 31, 1969. Discussion received after the closing date will be returned. Manuscript received by ASME Applied Mechanics Division, February 6, 1969; final revision, April 24, 1969. Paper No. 69-APMW-12.

## Nomenclature

$\mathbf{x}$ = position vector
$x, y, z$ = Cartesian coordinates
$r, \theta, z$ = cylindrical coordinates
$\xi, y, z$ = load centered coordinates
$\rho$ = spherical radius
$n$ = radial measure from $x$-axis
$u_x, u_y, u_z$ = displacements, Cartesian components
$p$ = Laplace transform variable
$\lambda, \mu$ = Lamé constants
$c_d, c_s$ = body wave speeds
$c_R$ = Rayleigh surface wave speed
$c$ = load speed
$l$ = ratio of body wave speeds
$\gamma$ = ratio of dilatational wave speed to load speed

*(Continued on next page)*

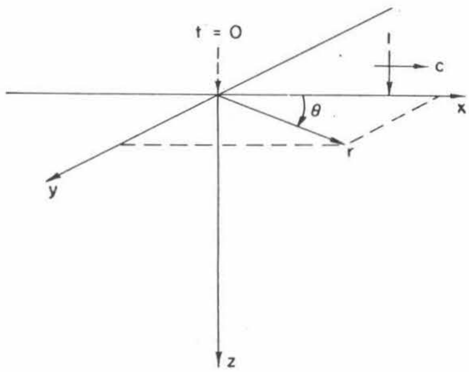


**Fig. 1 Traveling point load problem**

## 2 Formulation of Problem

The subject half-space problem is depicted in Fig. 1 based on a Cartesian coordinate system $(x, y, z)$. The plane surface of the half space is $z = 0$, with $z > 0$ forming the interior. A concentrated normal load of unit magnitude travels on the surface along the positive $x$-axis at a constant speed $c$. The load acquires its velocity instantaneously at the origin of the coordinates at time $t = 0$.

The half space is a homogeneous, isotropic medium governed by the equations of the linear theory of elasticity. The equations of motion for the case of vanishing body forces can be taken as the wave equations

$$\nabla^2\phi = \frac{1}{c_d^2}\frac{\partial^2\phi}{\partial t^2}, \qquad \nabla^2\boldsymbol{\psi} = \frac{1}{c_s^2}\frac{\partial^2\boldsymbol{\psi}}{\partial t^2} \tag{1}$$

where $\phi$ and $\boldsymbol{\psi}$, known as the Lamé potentials, are related to the displacement vector $\mathbf{u}$ by

$$\mathbf{u} = \nabla\phi + \nabla \times \boldsymbol{\psi} \tag{2}$$

and satisfy the divergence condition

$$\nabla \cdot \boldsymbol{\psi} = 0. \tag{3}$$

The constants $c_d$ and $c_s$, defined by $c_d^2 = (\lambda + 2\mu)/\nu$ and $c_s^2 = \mu/\nu$, represent the dilatational and equivoluminal body wave speeds, respectively, where $\lambda$ and $\mu$ are the Lamé constants and $\nu$ is the material density. The stresses $\tau_{ij}$ are related to the displacements by

$$\tau_{ij} = \lambda u_{k,k}\delta_{ij} + \mu(u_{i,j} + u_{j,i}), \tag{4}$$

where tensor notation is employed.

The boundary conditions at $z = 0$ take the form

$$\begin{aligned} \tau_{zz}(x, y, 0, t) &= -\delta(y)\delta(x - ct) \\ \tau_{xz}(x, y, 0, t) &= \tau_{yz}(x, y, 0, t) = 0, \end{aligned} \tag{5}$$

where $\delta$ is the Dirac delta function. To represent quiescence at $t = 0$, the initial conditions appear as

$$\phi(x, y, z, 0) = \frac{\partial\phi(x, y, z, 0)}{\partial t} = \boldsymbol{\psi}(x, y, z, 0) = \frac{\partial\boldsymbol{\psi}(x, y, z, 0)}{\partial t} = 0. \tag{6}$$

Finally, the potentials $\phi$ and $\boldsymbol{\psi}$, and the space derivatives of the potentials, are required to vanish at infinity.

## 3 Formal Solution

A solution of the wave equations (1) that satisfies the initial conditions (6) and the boundedness condition at infinity can be computed by using the Laplace and double Fourier transforms to suppress the time parameter and the $x, y$ space coordinates. Then satisfying the boundary conditions (5), using the displacement-potential relation (2), and inverting the Fourier transform give the Laplace transformed displacements as

$$\bar{u}_j(x, y, z, p) = \bar{u}_{jd}(x, y, z, p) + \bar{u}_{js}(x, y, z, p) \tag{7}$$

for $j = x, y, z$, where

$$\bar{u}_{j\alpha}(x, y, z, p) = \frac{1}{(2\pi)^2\mu}\iint_{-\infty}^{\infty} F_{j\alpha}(k, v, p)e^{-n_\alpha z + i(kx + vy)}\,dk\,dv \tag{8}$$

for $\alpha = d, s$, in which

$$\begin{aligned} F_{xd}(k, v, p) &= -ikn_0G, & F_{xs}(k, v, p) &= 2ikn_dn_sG \\ F_{yd}(k, v, p) &= -ivn_0G, & F_{ys}(k, v, p) &= 2ivn_dn_sG \\ F_{zd}(k, v, p) &= n_dn_0G, & F_{zs}(k, v, p) &= -2n_d(k^2 + v^2)G \end{aligned} \tag{9}$$

$$G = \frac{1}{(p + ick)T}, \tag{10}$$

$$T = n_0^2 - 4n_sn_d(k^2 + v^2), \tag{11}$$

$$n_d = (k^2 + v^2 + k_d^2)^{1/2}, \qquad n_s = (k^2 + v^2 + k_s^2)^{1/2}, \qquad n_0 = [k_s^2 + 2(k^2 + v^2)], \tag{12}$$

$$k_d = \frac{p}{c_d}, \qquad k_s = \frac{p}{c_s}, \tag{13}$$

$\bar{u}_j$ and $u_j$ are Laplace transform pairs, $p$ is the Laplace transform parameter, $k$ and $v$ are the Fourier transform parameters, and the square roots $n_d$ and $n_s$ are assigned the branch that has the positive, real part. In this form $\bar{u}_j$ is expressed as the sum of the dilatational contribution $\bar{u}_{jd}$ and an equivoluminal contribution $\bar{u}_{js}$.

## Nomenclature

- $\gamma_R$ = ratio of dilatational wave speed to Rayleigh wave speed
- $Q_d^\pm, Q_s^\pm, Q_c^\pm, Q_R^\pm$ = singularities in the $q$-plane
- $S_d^\pm, S_s^\pm, S_R^\pm, \mathcal{S}_d^\pm, \mathcal{S}_s^\pm, \mathcal{S}_R^\pm$ = singularities in the $w$-plane
- $q_d, q_s, q_{sd}$ = transformations in the $q$-plane
- $w_d, w_s, w_{sd}$ = transformations in the $w$-plane
- $t$ = time
- $t_d, t_s, t_{sd}, t_{dc}, t_{sc}, t_{sdc}$ = arrival times of waves
- $t_L, t_B, t_E, t_{sdc}^0$ = characteristic times in solution (not arrival times)
- $T_d, T_s, T_{sd}, A_{sd}$ = limits of integration
- H = Heaviside function
- $\phi_c$ = head wave angle

*Subscripts*

- $c$ = pertaining to moving load
- $d$ = pertaining to dilatational contribution
- $s$ = pertaining to equivoluminal contribution
- R = pertaining to Rayleigh surface wave
- $x, y, z$ = pertaining to displacement components

bold face characters indicate vectors

## 4 Inversion

The Laplace transform is inverted by a modification of Cagniard's [10] technique due to deHoop [11]. This technique consists of converting each $\bar{u}_{j\alpha}$ into the Laplace transform of a known function, and then inverting the Laplace transform by inspection. In the subsequent calculations $p$ is assumed to be a real, positive number. For such values of $p$, Lerch's theorem (see Carslaw and Jaeger [13]) guarantees that if $u_{j\alpha}$ exists, it is unique.

To simplify the form of $\bar{u}_{j\alpha}$, the transformations

$$k = \frac{p}{c_d}\beta, \qquad v = \frac{p}{c_d}\sigma \tag{14}$$

and

$$\beta = q\cos\theta - w\sin\theta, \qquad \sigma = q\sin\theta + w\cos\theta \tag{15}$$

are substituted successively into (8), yielding

$$\bar{u}_{j\alpha}(r, \theta, z, p) = \frac{1}{2}\int_0^\infty \int_{-\infty}^\infty K_{j\alpha}(q, w, \theta) e^{-\frac{p}{c_d}(m_\alpha z - iqr)}\, dq\, dw, \tag{16}$$

where

$$K_{xd}(q, w, \theta) = -[iq\cos\theta(iq\cos\theta + \gamma) + w^2\sin^2\theta]m_0L, \tag{17a}$$

$$K_{xs}(q, w, \theta) = 2[iq\cos\theta(iq\cos\theta + \gamma) + w^2\sin^2\theta]m_dm_sL, \tag{17b}$$

$$K_{yd}(q, w, \theta) = -\sin\theta[iq(iq\cos\theta + \gamma) - w^2\cos\theta]m_0L, \tag{17c}$$

$$K_{ys}(q, w, \theta) = 2\sin\theta[iq(iq\cos\theta + \gamma) - w^2\cos\theta]m_dm_sL, \tag{17d}$$

$$K_{zd}(q, w, \theta) = (iq\cos\theta + \gamma)m_0m_dL, \tag{17e}$$

$$K_{zs}(q, w, \theta) = -2(iq\cos\theta + \gamma)(q^2 + w^2)m_dL, \tag{17f}$$

$$L = \frac{1}{\pi^2 c\mu[(iq\cos\theta + \gamma)^2 + w^2\sin^2\theta]\mathrm{R}}, \tag{18}$$

$$\mathrm{R} = m_0^2 - 4m_dm_s(q^2 + w^2), \tag{19}$$

$$m_d = (q^2 + w^2 + 1)^{1/2}, \qquad m_s = (q^2 + w^2 + l^2)^{1/2}, \qquad m_0 = [l^2 + 2(q^2 + w^2)], \tag{20}$$

$$l = \frac{c_d}{c_s}, \qquad \gamma = \frac{c_d}{c}, \tag{21}$$

and $(r, \theta, z)$ are the cylindrical coordinates shown in Fig. 1. The transformation in (15) was introduced by deHoop [11] in order to simplify Cagniard's technique.

In view of the symmetry properties

$$\left.\begin{aligned} \bar{u}_{x\alpha}(r, \theta, z, p) &= \bar{u}_{x\alpha}(r, -\theta, z, p) \\ \bar{u}_{y\alpha}(r, \theta, z, p) &= -\bar{u}_{y\alpha}(r, -\theta, z, p) \\ \bar{u}_{z\alpha}(r, \theta, z, p) &= \bar{u}_{z\alpha}(r, -\theta, z, p), \end{aligned}\right\} \tag{22}$$

$\bar{u}_{j\alpha}$, and hence $\bar{u}_j$, are only inverted for $0 \leq \theta \leq \pi$. Since $u_{j\alpha}$ has different forms depending on the speed of the load relative to the body wave speeds, the inversion of each $\bar{u}_{j\alpha}$ is separated into three cases. In particular, the terms supersonic, transonic, and subsonic refer to the cases when the load speed is greater than the dilitational wave speed ($c > c_d$), between the dilatational and equivoluminal wave speeds ($c_d > c > c_s$), and less than the equivoluminal wave speed ($c < c_s$), respectively. In the remainder of this section $\bar{u}_{zd}$ and $\bar{u}_{zs}$ are inverted for the interior of the half space ($z > 0$) and for all load speeds ($0 \leq c < \infty$). Then $u_{zd}$ and $u_{zs}$ are combined to give $u_z$, and similar results are displayed for $u_x$ and $u_y$.

### Dilatational Contribution for Supersonic Load Motion

From (16)

$$\bar{u}_{zd}(\mathbf{x}, p) = \frac{1}{2}\int_0^\infty \int_{-\infty}^\infty K_{zd}(q, w, \theta) e^{-\frac{p}{c_d}(m_dz - iqr)}\, dq\, dw, \tag{23}$$

where $\mathbf{x}$ is the position vector. $\bar{u}_{zd}$ is converted into the Laplace transform of a known function by mapping $(1/c_d)(m_dz - iqr)$ into $t$ through a contour integration in a complex $q$-plane. To this end, the singularities of the integrand of $\bar{u}_{zd}$ are branch points at $q = Q_d^\pm$ and $q = Q_s^\pm$, and simple poles at $q = Q_c^\pm$ and $q = Q_R^\pm$, where

$$Q_d^\pm = \pm i(w^2 + 1)^{1/2}, \qquad Q_s^\pm = \pm i(w^2 + l^2)^{1/2}$$
$$Q_c^\pm = \frac{\pm w\sin\theta + i\gamma}{\cos\theta}, \qquad Q_R^\pm = \pm i(w^2 + \gamma_R^2)^{1/2}. \tag{24}$$

The poles at $q = Q_R^\pm$ correspond to the zeros of the Rayleigh function R, where $\gamma_R = c_d/c_R$ and $c_R$ is the Rayleigh surface wave speed. The roots of these singularities which lie in the upper half of the $q$-plane are shown in Fig. 2.

By seeking a particular contour in the $q$-plane such that

$$t = \frac{1}{c_d}(m_dz - iqr) \tag{25}$$

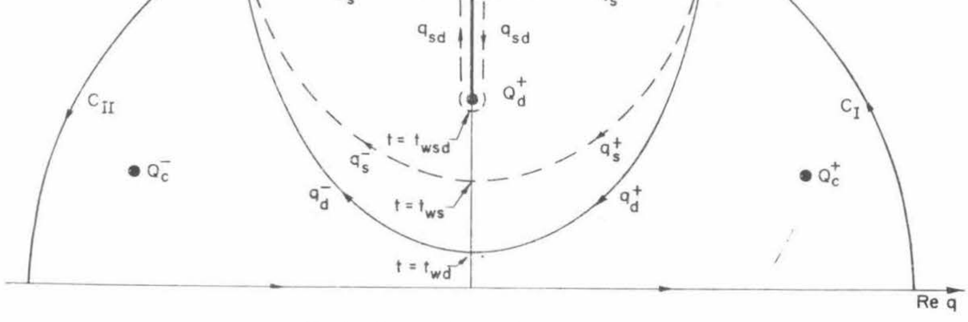


Fig. 2 Contour integration in the q-plane

one finds, upon solving for $q$, that

$$q = q_d^{\pm} = \frac{c_d}{\rho^2}\,[itr \pm z(t^2 - t_{wd}^2)^{1/2}] \tag{26}$$

for $t \geq t_{wd}$, where

$$t_{wd} = \frac{\rho}{c_d}\,(w^2 + 1)^{1/2}, \qquad \rho = (r^2 + z^2)^{1/2}. \tag{27}$$

Equation (26) defines one branch of a hyperbola with vertex $q = i(w^2 + 1)^{1/2} r/\rho$ and asymptotes $\arg q = \pm r/z$. As shown in Fig. 2 by a solid line labeled with $q_d^+$ and $q_d^-$, this hyperbola is parametrically described by $t$ as $t$ varies from $t_{wd}$ toward infinity. Since $r/\rho < 1$, the hyperbola does not intersect the branch cuts in the $q$-plane. The arcs $C_{\mathrm{I}}$ and $C_{\mathrm{II}}$ are introduced as shown in Fig. 2 to form a closed contour $C$, where $C =$ Re $q$-axis $+ C_{\mathrm{I}} + q_d^+ + q_d^- + C_{\mathrm{II}}$.

The poles at $q = Q_c^{\pm}$ lie inside $C$ if, and only if,

$$(1) \qquad -\frac{\pi}{2} < \theta < \frac{\pi}{2} \qquad (\text{or} \quad x > 0)$$

$$(2) \qquad \frac{c_d t r}{\rho^2} > \frac{\gamma}{\cos\theta} \qquad \left(\text{or} \quad t > t_L, \quad \text{where} \quad t_L = \frac{\rho^2}{cx}\right) \tag{28}$$

$$(3) \qquad w \tan\theta > \frac{z c_d}{\rho^2}\,(t^2 - t_{wd}^2)^{1/2}$$

For fixed $t$ and $z > 0$, $t = t_L$ defines the surface of a hemisphere with center $(x = ct/2,\ n = 0)$ and radius $ct/2$. Conditions (2) and (3) are equivalent to the condition $w^2 > w_{0d}^2$, where $w_{0d}^2 = (\rho^2\gamma^2 - x^2)z^2/r^2n^2$ and $n = (y^2 + z^2)^{1/2}$. To incorporate these conditions into the contour integration for $\bar{u}_{zd}$, the half space is separated into three regions:

**Region I:** $x > 0,\ \dfrac{x}{\rho} > \dfrac{c_d}{c}$ no appf.

The poles at $q = Q_c^{\pm}$ lie inside $C$ for $w \in [0, \infty)$.

**Region II:** $x > 0,\ \dfrac{x}{\rho} < \dfrac{c_d}{c}$ $0 < x < \infty$

The poles at $q = Q_c^{\pm}$ lie inside $C$ for $w \in (w_{0d}, \infty)$ and they lie outside $C$ for $w \in [0, w_{0d})$. (29)

**Region III:** $x < 0$

No poles lie inside $C$ for $w \in [0, \infty)$.

For $x > 0$, the rays $x/\rho = c_d/c$ form the surface of a cone whose axis is the positive $x$-axis. This conical surface is shown in Fig. 3(*a*) along with the part of $t = t_L$ which is bounded by $x/\rho < c_d/c$ and Roman numerals which depict the location of these regions in the half space (each Roman numeral lies between the rays that define the corresponding region). The next step is to invert $\bar{u}_{zd}$ for each of these regions.

**Region I.** The Cauchy-Goursat theorem and residue theory applied to the integrand of $\bar{u}_{zd}$ and $C$ yield

$$\bar{u}_{zd}(\mathbf{x}, p) = \bar{A}_{zd}(\mathbf{x}, p) + \overline{B}_{zd}(\mathbf{x}, p), \tag{30}$$

where

$$\bar{A}_{zd}(\mathbf{x}, p) = \int_0^{\infty}\int_{t_{wd}}^{\infty} \mathrm{Re}\left[K_{zd}(q_d, w, \theta)\,\frac{dq_d}{dt}\right] e^{-pt}\,dt\,dw \tag{31}$$

and

$$\overline{B}_{zd}(\mathbf{x}, p) = \mathrm{Re}\int_0^{\infty}\left[\hat{K}_{zd}(q, w, \theta) e^{-\frac{p}{c_d}(m_d z - iqr)}\right]\Bigg|_{q = c^+} dw, \tag{32}$$

in which

$$\hat{K}_{zd}(q, w, \theta) = \frac{\sec\theta}{\pi c \mu \mathrm{R}}\, m_d m_0. \tag{33}$$

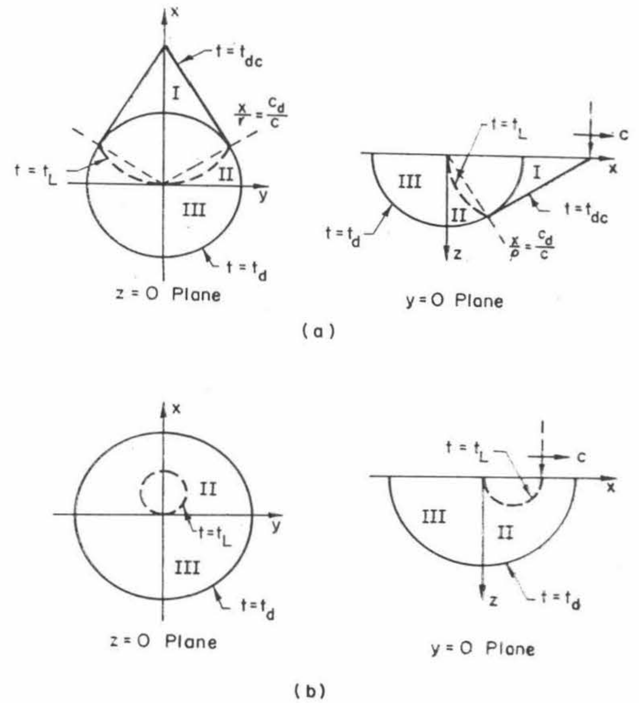


**Fig. 3 Dilatational wave pattern for (a) supersonic load motion and (b) transonic and subsonic load motion**

$\bar{A}_{zd}$ is the contribution from $q_d^{\pm}$, where $q_d = q_d^+$, and $\overline{B}_{zd}$ is the residue contribution from the poles at $q = Q_c^{\pm}$. The integrals that arise along $C_{\mathrm{I}}$ and $C_{\mathrm{II}}$ vanish as these contours recede to infinity.

By interchanging the order of integration in (31) and inverting the Laplace transform, one finds

$$A_{zd}(\mathbf{x}, t) = \mathrm{H}(t - t_d)\int_0^{T_d} \mathrm{Re}\left[K_{zd}(q_d, w, \theta)\,\frac{dq_d}{dt}\right] dw, \tag{34}$$

where

$$T_d = \left(\frac{t^2}{t_d^2} - 1\right)^{1/2}, \qquad t_d = \frac{\rho}{c_d}, \tag{35}$$

and H is the Heaviside function. $A_{zd}$ is a hemispherical, dilatational wave in that it represents the disturbance behind the wave front at $t = t_d$, where $t_d$ is the arrival time of a hemispherical, dilatational wave. This wave emanates from the initial position of the load as shown[4] in Fig. 3(*a*).

The inversion of $\overline{B}_{zd}$ is also done by a Cagniard technique. The singularities in the integrand of $\overline{B}_{zd}$ are shown in Fig. 4 with branch points at $w = S_d^{\pm}$ and $w = S_s^{\pm}$, and simple poles at $w = S_R^{\pm}$, where

$$\begin{aligned} S_d^{\pm} &= -i\gamma\sin\theta \pm i(1 - \gamma^2)^{1/2}\cos\theta \\ S_s^{\pm} &= -i\gamma\sin\theta \pm i(l^2 - \gamma^2)^{1/2}\cos\theta \\ S_R^{\pm} &= -i\gamma\sin\theta \pm i(\gamma_R^2 - \gamma^2)^{1/2}\cos\theta. \end{aligned} \tag{36}$$

In Fig. 4, the convention is adopted that $S_\alpha^{\pm}$ and $\mathcal{S}_\alpha^{\pm}$ represent roots of the same function, but whose positions are $w = S_\alpha^{\pm}$ for $c > c_\alpha$ and $w = \mathcal{S}_\alpha^{\pm}$ for $c < c_\alpha$, where $\alpha = d, s$, R. Here, since $c > c_d$, only the $S_\alpha^{\pm}$ arise and the $\mathcal{S}_\alpha^{\pm}$ are given later in the text. The poles at $w = S_R^{\pm}$ correspond to the roots of the Rayleigh function R in which $q = Q_c^+$.

[4] Arrival times are designated in the text by $t$ subscripted with lower case letters, and wave fronts are shown in the figures by solid lines.

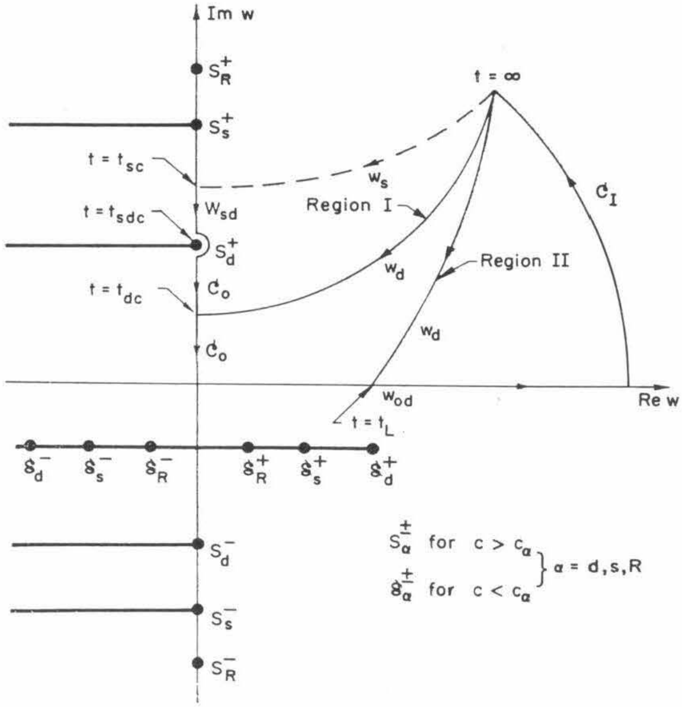


**Fig. 4 Contour integration in the w-plane**

The particular contour in the $w$-plane is given by

$$t = \frac{1}{c_d} (m_d z - iqr)\big|_{q=Q_c^+}, \tag{37}$$

or solving for $w$

$$w = w_d^\pm = -i\gamma \sin\theta + \frac{\gamma \cos\theta}{n^2} (i\xi y \pm z\alpha_d) \tag{38}$$

for $t \geq t_{dc}$, where

$$t_{dc} = \frac{1}{c}\left[\left(\frac{c^2}{c_d^2} - 1\right)^{1/2} n + x\right]$$

$$\alpha_d = \left[\xi^2 - \left(\frac{c^2}{c_d^2} - 1\right) n^2\right]^{1/2} \tag{39}$$

$$\xi = ct - x.$$

Equation (38) defines one branch of a hyperbola with vertex $w = -i\gamma \sin\theta + i(y/n)(1-\gamma^2)^{1/2}\cos\theta$ and asymptotes arg $w = \pm y/z$. In view of the limits of integration in (32), only the plus root of (38) is needed and $w_d = w_d^+$. As shown in Fig. 4 by the solid contour labeled for region I, the $w_d$ part of the hyperbola is parametrically described by $t$ as $t$ varies from $t_{dc}$ toward infinity. Since $x/\rho > c_d/c$ and $y/n < 1$, $w_d$ intersects the imaginary $w$-axis below the branch point at $w = S_d^+$ and above the real $w$-axis. As shown in Fig. 3($a$), $t_{dc}$ represents the arrival time of a conical, dilatational wave which trails behind the load.

The contours $\mathcal{C}_0$ and $\mathcal{C}_I$ are introduced as shown in Fig. 4 to form a closed contour which includes $w_d$ and the real $w$-axis. Then the application of the Cauchy-Goursat theorem to the integrand of $\overline{B}_{zd}$ and this closed contour produces, upon inverting the Laplace transform,

$$B_{zd}(\mathbf{x}, t) = \mathrm{Re}\left[\hat{K}_{zd}(w_d, \theta)\frac{dw_d}{dt}\right] \mathrm{H}(t - t_{dc}), \tag{40}$$

where

$$\hat{K}_{zd}(w, \theta) = \hat{K}_{zd}(Q_c^+, w, \theta). \tag{41}$$

The integral that arises along $\mathcal{C}_I$ vanishes as $\mathcal{C}_I$ recedes to infinity and the one along $\mathcal{C}_0$ vanishes because its real part is zero. Finally, $B_{zd}$ represents a conical, dilatational wave trailing behind the load.

The sum of $A_{zd}$ and $B_{zd}$ gives $u_{zd}$ for region I as

$$u_{zd}(\mathbf{x}, t) = \mathrm{H}(t - t_d)\int_0^{T_d} \mathrm{Re}\left[K_{zd}(q_d, w, \theta)\frac{dq_d}{dt}\right] dw$$
$$+ \mathrm{Re}\left[\hat{K}_{zd}(w_d, \theta)\frac{dw_d}{dt}\right]\mathrm{H}(t - t_{dc}). \tag{42}$$

**Region II.** By noting the conditions for region II in (29) and completing the contour integration in the $q$-plane, one finds

$$\bar{A}_{zd}(\mathbf{x}, p) = \int_0^\infty P\int_{t_{wd}}^\infty \mathrm{Re}\left[K_{zd}(q_d, w, \theta)\frac{dq_d}{dt}\right]e^{-pt}dt\, dw \tag{43}$$

and

$$\overline{B}_{zd}(\mathbf{x}, p) = \mathrm{Re}\int_{w_{0d}}^\infty \left[\hat{K}_{zd}(q, w, \theta)e^{-\frac{p}{c_d}(m_d z - iqr)}\right]\Bigg|_{q=Q_c^+} dw, \tag{44}$$

where $\bar{u}_{zd}$ is the sum of $\bar{A}_{zd}$ and $\overline{B}_{zd}$. The letter $P$ precedes an improper integral to imply that it is interpreted in the sense of a Cauchy principal value. Such an integral arises in $\bar{A}_{zd}$ because the poles at $q = Q_c^\pm$ coalesce on $q_d^\pm$ at $t = t_L$ as $w \to w_{0d}$. Beyond this, $\bar{A}_{zd}$ is exactly the same as for region I, while $\overline{B}_{zd}$ only differs in the lower limit, which is expected since the poles at $q = Q_c^\pm$ only lie inside $C$ for $w > w_{0d}$.

The inversion of $\overline{B}_{zd}$ proceeds as for region I, but with modifications in the geometry of the $w$-plane. For region II the particular contour $w_d$ intersects the real $w$-axis as shown in Fig. 4, to comply with the limits of integration in $\overline{B}_{zd}$. Furthermore, the singularities $S_d^+$, $S_s^+$, and $S_R^+$ may lie below the real $w$-axis, but still on the imaginary $w$-axis, in a manner which is not shown in Fig. 4. However, since the particular contour does not intersect the imaginary $w$-axis, this has no bearing on the contour integration for region II. Then inverting $\bar{A}_{zd}$ and $\overline{B}_{zd}$ and combining the results give $u_{zd}$ for region II as

$$u_{zd}(\mathbf{x}, t) = \mathrm{H}(t - t_d)P \int_0^{T_d} \mathrm{Re}\left[K_{zd}(q_d, w, \theta)\frac{dq_d}{dt}\right] dw + \mathrm{Re}\left[\hat{K}_{zd}(w_d, \theta)\frac{dw_d}{dt}\right]\mathrm{H}(t - t_L). \quad (45)$$

The first term in $u_{zd}$ represents a hemispherical, dilatational wave as for region I. However, for region II, the integral is interpreted as a Cauchy principal value for $t = t_L$. The second term has the same algebraic form as for region I, but the conical wave front is replaced with the hemispherical surface $t = t_L$. This new surface is not expected to be a wave front (i.e., $u_{zd}$ and all the derivatives of $u_{zd}$ are expected to be continuous through $t = t_L$) because it is not a characteristic surface (similar to $t = t_d$), or the closure of characteristic surfaces (similar to $t = t_{dc}$), associated with the governing wave equation for the dilatational potential $\phi$ in (1).

**Region III.** As indicated in (29) for region III no poles lie inside $C$. Therefore, the inversion of $\bar{u}_{zd}$ proceeds exactly as for region I, less the residue term $\overline{B}_{zd}$, and $u_{zd}$ can be obtained from (42) by deleting the algebraic term.

**Summary.** By comparing the results for each region it follows that $u_{zd}$ can be represented by one expression for all three regions; namely,

$$u_{zd}(\mathbf{x}, t) = \mathrm{H}(t - t_d)P \int_0^{T_d} \mathrm{Re}\left[K_{zd}(q_d, w, \theta)\frac{dq_d}{dt}\right] dw + \mathrm{Re}\left[\hat{K}_{zd}(w_d, \theta)\frac{dw_d}{dt}\right]\mathrm{H}(t - t_{dc})H(t - t_L)\mathrm{H}(x). \quad (46)$$

This expression is valid for $0 \leq \theta \leq \pi$ and $z > 0$. The wave pattern associated with $u_{zd}$ is shown in Fig. 3($a$), where the relationship between the rays $x/\rho = c_d/c$, the wave fronts $t = t_d$ and $t = t_{dc}$, the hemispherical surface $t = t_L$, and the regions I–III is depicted.

### Dilatational Contribution for Transonic and Subsonic Load Motion

The inversion of $\bar{u}_{zd}$ for $c_s < c < c_d$ and $c < c_s$, or equivalently $c < c_d$, proceeds exactly as for $c > c_d$, except that of the three regions in (29) only II and III are applicable for $c < c_d$ because $x/\rho$ is always less than $c_d/c$. These two regions are depicted in Fig. 3($b$) by Roman numerals two and three.

The inversion of $\bar{u}_{zd}$ for region II proceeds for $c < c_d$ as it did for $c > c_d$, except that the geometry of the $w$-plane is different. As shown in Fig. 4, the position of the singularities varies depending on the value of $c$ relative to $c_s$, $c_d$, and $c_R$. In that figure

$$\begin{aligned} \mathrm{S}_d^{\pm} &= -i\gamma \sin\theta \pm (\gamma^2 - 1)^{1/2}\cos\theta \\ \mathrm{S}_s^{\pm} &= -i\gamma \sin\theta \pm (\gamma^2 - l^2)^{1/2}\cos\theta \\ \mathrm{S}_R^{\pm} &= -i\gamma \sin\theta \pm (\gamma^2 - \gamma_R^2)^{1/2}\cos\theta. \end{aligned} \quad (47)$$

However, the particular contour in the $w$-plane for region II remains the same for all load speeds ($c > c_d$ and $c < c_d$), as does the result of a contour integration which includes it and the real $w$-axis. Therefore, $u_{zd}$ for region II and $c < c_d$ is the same as given for $c > c_d$ in (45). Furthermore, the inversion of $\bar{u}_{zd}$ for region III is independent of the value of the load speed (which only appears through the position of the poles at $q = Q_c^{\pm}$) and the result is the same as given for $c > c_d$. Then combining the results for regions II and III gives $u_{zd}$ for $c < c_d$ as

$$u_{zd}(\mathbf{x}, t) = \mathrm{H}(t - t_d)P \int_0^{T_d} \mathrm{Re}\left[K_{zd}(q_d, w, \theta)\frac{dq_d}{dt}\right] dw + \mathrm{Re}\left[\hat{K}_{zd}(w_d, \theta)\frac{dw_d}{dt}\right]\mathrm{H}(t - t_L)\mathrm{H}(x), \quad (48)$$

where $0 \leq \theta \leq \pi$ and $z > 0$. The dilatational wave pattern for $c < c_d$ is shown in Fig. 3($b$). As expected physically, the conical wave front does not exist, leaving only the hemispherical one.

Finally, by comparing (46) and (48) one finds that $u_{zd}$ is given by (46) for all load speeds if the Heaviside function satisfies the condition

$$\mathrm{H}(t - t_{dc}) = 1 \quad (49)$$

for $c < c_d$.

### Equivoluminal Contribution

The inversion of $\bar{u}_{zs}$ proceeds as for $\bar{u}_{zd}$, but $u_{zs}$ is more complicated than $u_{zd}$ due to the appearance of head waves (or von Schmidt waves).

With $\bar{u}_{zs}$ being given by (16) for $j = z$ and $\alpha = s$, the corresponding $q$-plane is shown in Fig. 2, where the singularities are the same as for $\bar{u}_{zd}$, but the particular contour has two possible configurations which are denoted by dashed lines. If $r/\rho < c_s/c_d$ and $w \in [0, \infty)$ or if $r/\rho > c_s/c_d$ and $w \in (w_1, \infty)$, where $w_1 = (r^2 l^2 - \rho^2)^{1/2}/z$, then the particular contour is similar to $q_d^{\pm}$ and it is denoted by $q_s^{\pm}$, where

$$q_s^{\pm} = \frac{c_d}{\rho^2}\,[itr \pm z(t^2 - t_{ws}^2)^{1/2}] \quad (50)$$

for $t \geq t_{ws}$, in which

$$t_{ws} = \frac{\rho}{c_d}\,(w^2 + l^2)^{1/2}. \quad (51)$$

However, if $r/\rho > c_s/c_d$ and $w \in [0, w_1)$, then the vertex of $q_s^{\pm}$ lies on the branch cut between the branch points at $q = Q_d^{+}$ and $q = Q_s^{+}$, and the particular contour is given by $q_s^{\pm}$ plus $q_{sd}$, where

$$q_{sd} = \frac{ic_d}{\rho^2}\,[tr - z(t_{ws}^2 - t^2)^{1/2}] \quad (52)$$

for $t_{ws} \geq t \geq t_{wsd}$, in which

$$t_{wsd} = \frac{1}{c_d}\,[(l^2 - 1)^{1/2}z + (w^2 + 1)^{1/2}r]. \quad (53)$$

As shown in Fig. 2, the closed contour $C$ now includes $q_s^{\pm}$, $q_{sd}$ when it arises, and the real $q$-axis. As for $\bar{u}_{zd}$, the poles at $q = Q_c^{\pm}$ can lie either inside or outside of $C$.

In regard to the various positions of the poles at $q = Q_c^{\pm}$ and the vertex of $q_s^{\pm}$, the inversion of $\bar{u}_{zs}$ is separated into seven cases, each of which corresponds to a particular region of the half space:

**Region I:** $x > 0, \dfrac{x}{\rho} > \dfrac{c_s}{c}, \dfrac{r}{\rho} < \dfrac{c_s}{c_d}, \dfrac{x}{r} > \dfrac{c_d}{c}$

The poles lie inside $C$ for $w \in [0, \infty)$.
The vertex does not lie on the branch cut for $w \in [0, \infty)$.

**Region II:** $x > 0, \dfrac{x}{\rho} > \dfrac{c_s}{c}, \dfrac{r}{\rho} > \dfrac{c_s}{c_d}, \dfrac{x}{r} > \dfrac{c_d}{c}$

The poles lie inside $C$ for $w \in [0, \infty)$.
The vertex lies on the branch cut for $w \in [0, w_1)$.

**Region III:** $x > 0, \dfrac{x}{\rho} > \dfrac{c_s}{c}, \dfrac{r}{\rho} > \dfrac{c_s}{c_d}, \dfrac{x}{r} < \dfrac{c_d}{c}$

The vertex lies on the branch cut for $w \in [0, w_1)$.
The poles lie inside $C$ for $w \in (0, \infty)$ and coalesce on $q_{sd}$ as $w \to 0$. The poles also coalesce on $q_{sd}$ as $\theta \to 0$ for $c_s < c < c_d$ and $w \in [0, (\gamma^2 - 1)^{1/2})$.

**Region IV:** $x > 0, \dfrac{x}{\rho} < \dfrac{c_s}{c}, \dfrac{r}{\rho} < \dfrac{c_s}{c_d}$

The poles lie inside $C$ for $w \in (w_{0s}, \infty)$.
The vertex does not lie on the branch cut for $w \in [0, \infty)$.

**Region V:** $x > 0, \dfrac{x}{\rho} < \dfrac{c_s}{c}, \dfrac{r}{\rho} > \dfrac{c_s}{c_d}$

The poles lie inside $C$ for $w \in (w_{0s}, \infty)$.
The vertex lies on the branch cut for $w \in [0, w_1)$.

The poles coalesce on $q_{sd}$ as $\theta \to 0$ for $c < c_d$ and $w \in (w_{0s}, (\gamma^2 - 1)^{1/2})$.

**Region VI:** $x < 0, \dfrac{r}{\rho} < \dfrac{c_s}{c_d}$

No poles lie inside $C$ for $w \in [0, \infty)$.
The vertex does not lie on the branch cut for $w \in [0, \infty)$.

**Region VII:** $x < 0, \dfrac{r}{\rho} > \dfrac{c_s}{c_d}$

No poles lie inside $C$ for $w \in [0, \infty)$.
The vertex lies on the branch cut for $w \in [0, w_1)$.

(Regions I–VII are referred to in the text by (54))

In (54), $w_{0s} = (\rho^2\gamma^2 - x^2l^2)^{1/2}z/rn$. For $x > 0$, the rays $x/\rho = c_s/c$ form the surface of a cone which is similar to $x/\rho = c_d/c$, and $x/r = c_d/c$ defines two planes, one for $\theta > 0$ and one for $\theta < 0$. Also, $r/\rho = c_s/c_d$ defines the surface of a cone whose axis is the positive $z$-axis. All seven regions arise when inverting $\bar{u}_{zs}$ for $c > c_d$, but only regions III–VII and regions IV–VII arise for $c_s < c < c_d$ and $c < c_s$, respectively. The Roman numerals in Figs. 5–8 depict the location of these regions in the half space.

By inverting $\bar{u}_{zs}$ for each region, accounting for the variable load speed, and combining the results, one finds

$$\begin{aligned}
u_{zs}(\mathbf{x}, t) = {} & \mathrm{H}(t - t_s)P \int_0^{T_s} \mathrm{Re}\left[K_{zs}(q_s, w, \theta)\frac{dq_s}{dt}\right] dw \\
& + \mathrm{H}(t - t_{sd})\mathrm{H}(t_B - t)\mathrm{H}\left(\frac{r}{\rho} - \frac{c_s}{c_d}\right) \\
& \times P\int_{A_{sd}}^{T_{sd}} \mathrm{Re}\left[K_{zs}(q_{sd}, w, \theta)\frac{dq_{sd}}{dt}\right] dw \\
& + \mathrm{Re}\left[\hat{K}_{zs}(w_s, \theta)\frac{dw_s}{dt}\right]\mathrm{H}(t - t_{sc})\mathrm{H}(t - t_L)\mathrm{H}(x) \\
& + \mathrm{Re}\left[\hat{K}_{zs}(w_{sd}, \theta)\frac{dw_{sd}}{dt}\right]\mathrm{H}\left(\frac{y}{n} - \phi_c\right) \\
& \times \left[\mathrm{H}(t - t_{sdc})\mathrm{H}\left(\frac{x}{r} - \frac{c_d}{c}\right)\right. \\
& + \mathrm{H}(t - t_E)\mathrm{H}\left(\frac{x}{\rho} - \frac{c_s}{c}\right)\mathrm{H}\left(\frac{c_d}{c} - \frac{x}{r}\right) \\
& \left. - \mathrm{H}(t - t_{sc})\mathrm{H}\left(\frac{x}{\rho} - \frac{c_s}{c}\right)\right]\mathrm{H}(x) \qquad (55)
\end{aligned}$$

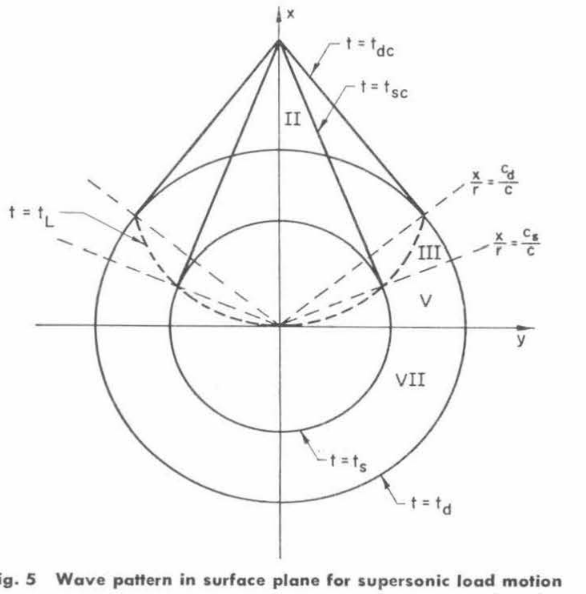


**Fig. 5 Wave pattern in surface plane for supersonic load motion**

for $0 \le \theta \le \pi$, $z > 0$, and $0 \le c < \infty$. Further details on inverting $\bar{u}_{zs}$ are given in a thesis by the first author [14]. The symbols in $u_{zs}$ which have not been previously defined are

$$\hat{K}_{zs}(w, \theta) = \frac{-2 \sec \theta}{\pi c \mu \mathrm{R}} m_d(q^2 + w^2)|_{q=Qc^+}, \qquad (56)$$

$$\begin{aligned}
w_s &= -i\gamma \sin \theta + \frac{\gamma \cos \theta}{n^2}(i\xi y + z\alpha_s) \\
w_{sd} &= -i\gamma \sin \theta + \frac{i\gamma \cos \theta}{n^2}(\xi y - z\alpha_{sd}),
\end{aligned} \qquad (57)$$

$$\alpha_s = \left[\xi^2 - \left(\frac{c^2}{c_s^2} - 1\right)n^2\right]^{1/2},$$

$$\alpha_{sd} = \left[\left(\frac{c^2}{c_s^2} - 1\right)n^2 - \xi^2\right]^{1/2}, \qquad (58)$$

$$A_{sd} = \begin{cases} 0 & \text{for} \quad t < t_s \\ T_s & \text{for} \quad t > t_s, \end{cases} \qquad (59)$$

$$T_s = \left(\frac{t^2}{t_s^2} - 1\right)^{1/2} l, \qquad T_{sd} = \left[\left(\frac{c_d(t - t_{sd})}{r} + 1\right)^2 - 1\right]^{1/2}, \qquad (60)$$

$$t_s = \frac{\rho}{c_s}, \qquad t_{sd} = \frac{1}{c_d}\left[(l^2 - 1)^{1/2}z + r\right],$$

$$t_B = \frac{\rho^2(l^2 - 1)^{1/2}}{zc_d}, \qquad t_E = \frac{1}{cx}\left[\left(\frac{c^2}{c_s^2}x^2 - r^2\right)^{1/2} z + r^2\right] \qquad (61)$$

$$t_{sc} = \frac{1}{c}\left[\left(\frac{c^2}{c_s^2} - 1\right)^{1/2} n + x\right],$$

$$t_{sdc} = \frac{1}{c}\left[\left(\frac{c^2}{c_s^2} - \frac{c^2}{c_d^2}\right)^{1/2} z + \left(\frac{c^2}{c_d^2} - 1\right)^{1/2} y + x\right],$$

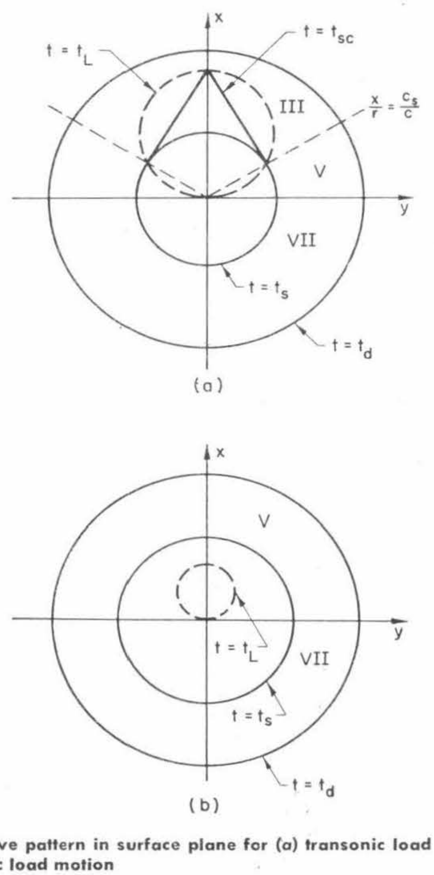


**Fig. 6 Wave pattern in surface plane for (a) transonic load motion and (b) subsonic load motion**

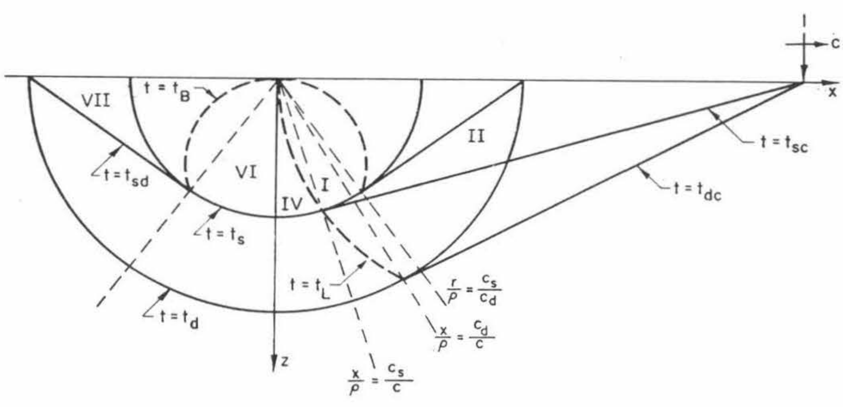


**Fig. 7 Wave pattern in plane under the path of load for supersonic load motion**

$$\phi_c = \frac{\left(\dfrac{c^2}{c_d^2} - 1\right)^{1/2}}{\left(\dfrac{c^2}{c_s^2} - 1\right)^{1/2}}. \tag{62}$$

The Heaviside function in (55) is restricted by the conditions

$$\begin{aligned} \mathrm{H}(t - t_{sc}) &= 1 \qquad \text{if } c < c_s \\ \mathrm{H}\left(\frac{y}{n} - \phi_c\right) &= 1 \qquad \text{if } c < c_d. \end{aligned} \tag{63}$$

The wave geometry associated with $u_{zs}$ is shown in Figs. 5–9. The dilatational wave fronts are included in these diagrams for reference; therefore, they display the wave geometry associated with the total displacement $u_z$. However, the Roman numerals in these diagrams only correspond to $u_{zs}$ and the regions described in (54).

The first and third terms in $u_{zs}$, which are analogous to the dilatational waves in $u_{zd}$, represent hemispherical and conical, equivoluminal waves, respectively. The second term in $u_{zs}$ is the contribution from $q_{sd}$ along the imaginary axis in the $q$-plane and it represents a head wave whose wave front is the surface of the truncated cone given by $t = t_{sd}$ for $r/\rho > c_s/c_d$. This wave, referred to as the conical head wave, is generated by the surface intersection of the dilatational wave front at $t = t_d$ and it propagates in front of $t = t_B$, as shown in Figs. 7 and 8($a$, $b$); thereby, contributing both ahead and behind the equivoluminal wave front at $t = t_s$ for $r/\rho > c_s/c_d$. For fixed time, $t = t_B$ is the surface of a sphere with center ($r = 0$, $z = c_d t/2(l^2 - 1)^{1/2}$) and radius $c_d t/2(l^2 - 1)^{1/2}$. The surface $t = t_B$ is not expected to be a wave front because it is not a characteristic surface, or the closure of characteristic surfaces, of the wave equation for the equivoluminal potential $\boldsymbol{\psi}$ in (1).

The integral in the second term of $u_{zs}$ is improper for $t = t_s$ because its integrand contains a first-order singularity at $w = 0$ (i.e., its integrand behaves like $1/w$ as $w \to 0$). This singularity is introduced by the differential of $q_{sd}$. In section 5 this integral is evaluated for $t \to t_s$, displaying a logarithmic singularity in $u_{zs}$ for $t = t_s$. This integral is also improper for certain points in the plane under the path of the load (the $\theta = 0$-plane). In particular, it is interpreted as a Cauchy principal value for $t_{sc} < t < t_{sdc}^0$ if $\theta = 0$, $x/\rho > c_s/c$, and $c_s < c < c_d$; and for $t_L < t < t_{sdc}^0$ if $\theta = 0$, $x/\rho < c_s/c$, and $c < c_d$, where $t_{sdc}^0$ equals $t_{sdc}$ evaluated for $\theta = 0$ and $t = t_{sdc}^0$ is shown in Fig. 8($a$, $b$) by a dashed line projecting out from the load. The improper integral for $\theta = 0$ reflects the way the poles at $q = Q_c^{\pm}$ coalesce on $q_{sd}$ as $\theta \to 0$, and as described in (54) for regions III and V. Furthermore, if the Cauchy principal value is evaluated for $\theta \to 0$, it combines with the remaining terms in $u_{zs}$ to render $u_{zs}$ continuous as $\theta \to 0$, which is expected physically.

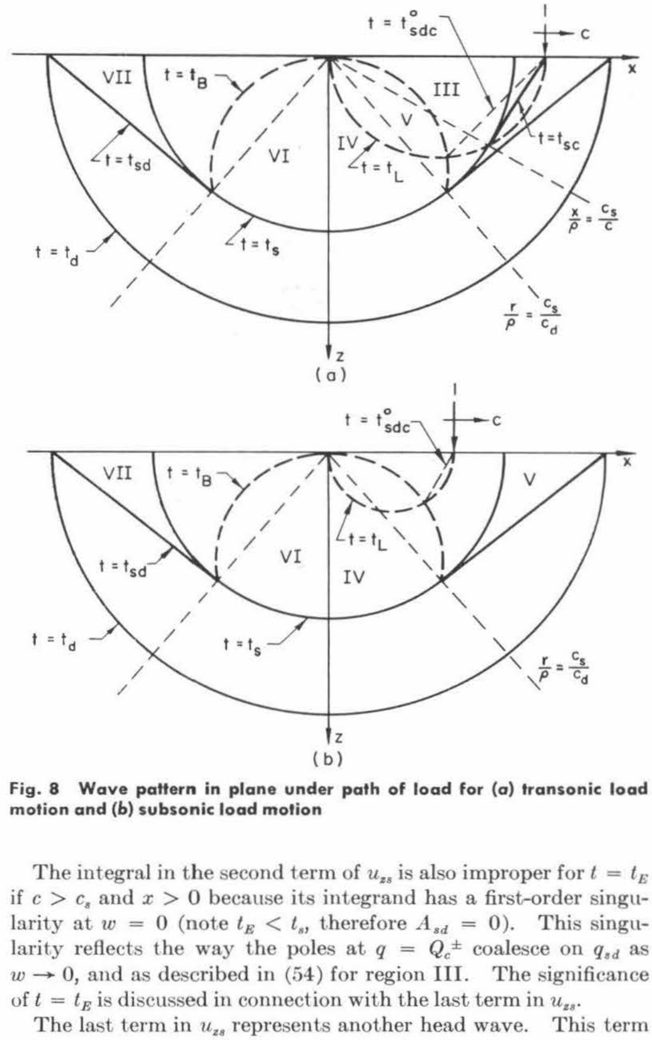


**Fig. 8 Wave pattern in plane under path of load for (a) transonic load motion and (b) subsonic load motion**

The integral in the second term of $u_{zs}$ is also improper for $t = t_E$ if $c > c_s$ and $x > 0$ because its integrand has a first-order singularity at $w = 0$ (note $t_E < t_s$, therefore $A_{sd} = 0$). This singularity reflects the way the poles at $q = Q_c^{\pm}$ coalesce on $q_{sd}$ as $w \to 0$, and as described in (54) for region III. The significance of $t = t_E$ is discussed in connection with the last term in $u_{zs}$.

The last term in $u_{zs}$ represents another head wave. This term is the contribution from the contour $w_{sd}$ which is indicated in Fig. 4 as a segment of the imaginary $w$-axis. The dashed contour that is shown in this figure along with $w_{sd}$ is the particular contour which arises in the $w$-plane for $\bar{u}_{zs}$ and region II if $y/n > \phi_c$ (the rays $y/n = \phi_c$ are shown in Fig. 9). This particular contour has other configurations for region II if $y/n < \phi_c$ (in this case the $w_{sd}$ segment does not arise), and for the other regions in (54), but they are not displayed here.

This second head wave has a plane surface for a wave front which is given by $t = t_{sdc}$ for $y/n > \phi_c$ and $x/r > c_d/c$. This

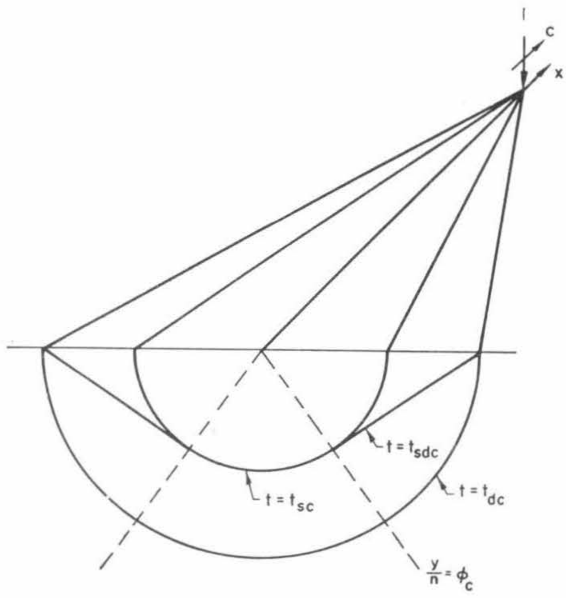


**Fig. 9 Waves trailing behind load for supersonic load motion**

wave, referred to as the plane head wave, only exists for $c > c_d$ and then it is generated by the surface intersection of the dilatational wave front at $t = t_{dc}$ and it propagates in front of $t = t_{sc}$, as shown in Fig. 9. For $x/r = c_d/c$ the plane head wave front is tangent to the conical head wave front and for $x/r < c_d/c$ it does not exist because its generator, $t = t_{dc}$, does not exist, as shown in Fig. 5. In the region bounded by $x/r < c_d/c$ and $x/\rho > c_s/c$ the plane head wave ends. This is reflected in $u_{zs}$ by the fact that the last term is discontinuous for $t = t_E$ and the integral in the second term is improper for $t = t_E$. The surface defined by $t = t_E$, which is not shown in any of the figures, is not expected to be a wave front for the same reason as just given for $t = t_B$.

For $c_s < c < c_d$, the plane head wave front does not exist, which can be seen in (55) since now $\mathrm{H}((x/r) - (c_d/c)) = 0$. Physically this is expected since its generator, $t = t_{dc}$, does not exist. In this case the last term in $u_{zs}$ still represents an equivoluminal disturbance propagating in front of $t = t_{sc}$. However, now it propagates behind the surface $t = t_E$, which is behind the conical head wave front at $t = t_{sd}$, and which makes the last term indistinguishable as a separate wave. Finally, for $c < c_s$ the last term does not contribute to $u_{zs}$, which can be seen in (55) since $H((x/r) - (c_d/c)) = 0$ and $\mathrm{H}((x/\rho) - (c_s/c)) = 0$.

### Total Displacement Field

The total disturbance comprising $u_z$ is the sum of $u_{zd}$ and $u_{zs}$. Similar expressions can be computed for $u_x$ and $u_y$, and all three displacements are written as

$$u_j(\mathbf{x}, t) = \sum_{\beta=1}^{6} u_{j\beta}(\mathbf{x}, t), \qquad (j = x, y, z) \tag{64}$$

for $0 \leq r < \infty$, $0 \leq \theta \leq \pi$ (or $-\infty < x < \infty$, $0 \leq y < \infty$), $0 < z < \infty$, and $0 \leq c < \infty$, where

$$u_{j1}(\mathbf{x}, t) = \mathrm{H}(t - t_d)P \int_0^{T_d} \mathrm{Re}\left[K_{jd}(q_d, w, \theta)\frac{dq_d}{dt}\right] dw, \tag{65}$$

$$u_{j2}(\mathbf{x}, t) = \mathrm{H}(t - t_s)P \int_0^{T_s} \mathrm{Re}\left[K_{js}(q_s, w, \theta)\frac{dq_s}{dt}\right] dw, \tag{66}$$

$$u_{j3}(\mathbf{x}, t) = \mathrm{H}(t - t_{sd})\mathrm{H}(t_B - t)\mathrm{H}\left(\frac{r}{\rho} - \frac{c_s}{c_d}\right) \times P \int_{A_{sd}}^{T_{sd}} \mathrm{Re}\left[K_{js}(q_{sd}, w, \theta)\frac{dq_{sd}}{dt}\right] dw, \tag{67}$$

$$u_{j4}(\mathbf{x}, t) = \mathrm{Re}\left[\hat{K}_{jd}(w_d, \theta)\frac{dw_d}{dt}\right]\mathrm{H}(t - t_{dc})\mathrm{H}(t - t_L)\mathrm{H}(x), \tag{68}$$

$$u_{j5}(\mathbf{x}, t) = \mathrm{Re}\left[\hat{K}_{js}(w_s, \theta)\frac{dw_s}{dt}\right]\mathrm{H}(t - t_{sc})\mathrm{H}(t - t_L)\mathrm{H}(x), \tag{69}$$

$$\begin{aligned} u_{j6}(\mathbf{x}, t) = \mathrm{Re}\left[\hat{K}_{js}(w_{sd}, \theta)\frac{dw_{sd}}{dt}\right]\mathrm{H}\left(\frac{y}{n} - \phi_c\right) &\times \left[\mathrm{H}(t - t_{sdc})\mathrm{H}\left(\frac{x}{r} - \frac{c_d}{c}\right)\right. \\ &+ \mathrm{H}(t - t_E)\mathrm{H}\left(\frac{x}{\rho} - \frac{c_s}{c}\right)\mathrm{H}\left(\frac{c_d}{c} - \frac{x}{r}\right) \\ &\left. - \mathrm{H}(t - t_{sc})\mathrm{H}\left(\frac{x}{\rho} - \frac{c_s}{c}\right)\right]\mathrm{H}(x). \end{aligned} \tag{70}$$

The symbols which have not been previously defined are

$$\hat{K}_{xd}(w, \theta) = \frac{\gamma \sec\theta}{\pi c \mu \mathrm{R}} m_0\Big|_{q=Q_c^+}, \tag{71}$$

$$\hat{K}_{xs}(w, \theta) = \frac{-2\gamma \sec\theta}{\pi c \mu \mathrm{R}} m_d m_s\Big|_{q=Q_c^+}, \tag{72}$$

$$\hat{K}_{yd}(w, \theta) = \frac{\sec^2\theta}{\pi c \mu \mathrm{R}} (\gamma \sin\theta - iw) m_0\Big|_{q=Q_c^+}, \tag{73}$$

$$\hat{K}_{ys}(w, \theta) = \frac{-2\sec^2\theta}{\pi c \mu \mathrm{R}} (\gamma \sin\theta - iw) m_d m_s\Big|_{q=Q_c^+}. \tag{74}$$

In this form the first three terms in $u_j$ represent a system of waves which emanate from the initial position of the load as if they were generated by a stationary point source. On the other hand, the last three terms represent disturbances that trail behind the load and whose wave geometry depends on the speed of the load relative to the body wave speeds.

Finally, it is noted that the interior displacements given here are not uniformly valid in $z$, as $z \to 0$, because the particular contours in the $q$ and $w$-planes wrap around the poles at $q = Q_R^+$ and $w = S_R^+$ as $z \to 0$. Therefore, to obtain the surface displacements it is necessary to return to the formal solution in (7) and (8), set $z = 0$, and then invert the displacements (or equivalently, evaluate the contribution of the poles at $q = Q_R^+$ and $w = S_R^+$ as $z \to 0$, and combine the results with the interior displacements in (64)–(70) evaluated for $z = 0$). However, since Payton [1] and Lansing [2] have already investigated the surface displacements, they are not displayed here; but they are given in [14] in context with the technique used here.

## 5 Wave-Front Expansions

The wave form of the solution given in (64)–(70) is advantageous for evaluating the displacements near the wave fronts. To facilitate these expansions for the waves emanating from the initial position of the load, the time-dependence in the limits of the integrals in (65)–(67) is removed by the transformation

$$w = [A^2 + (B^2 - A^2)\sin^2\alpha]^{1/2}, \tag{75}$$

where $A$ is the lower limit and $B$ is the upper limit of the particular integral in question, and the $\alpha$ range of integration is 0 to $\pi/2$. Furthermore, this transformation removes a half-order singularity in the integrands of $u_{j1}$ and $u_{j2}$ which is introduced by the differentials of $q_d$ and $q_s$. Then $u_{j1}$, $u_{j2}$, and $u_{j3}$ are evaluated as $t \to t_d$, $t \to t_s$, and $t \to t_{sd}$, respectively, by first expanding the appropriate integrands and then integrating these expansions from 0 to $\pi/2$. Special attention must be given to $u_{j3}$ since the integral in this term is improper for $t = t_s$. This term is evaluated by first approximating the improper integral for $t$ near $t_s$ and then letting $t \to t_s$. In this way, one finds

$$u_{j1} = A_{j1} + O(t - t_d) \quad \text{as} \quad t \to t_d, \tag{76}$$

$$u_{j2} = \begin{cases} A_{j2} + O(t - t_s) & \text{for} \quad \dfrac{r}{\rho} < \dfrac{c_s}{c_d} \\ A_{j2}' + O((t - t_s)^{1/2}) & \text{for} \quad \dfrac{r}{\rho} > \dfrac{c_s}{c_d} \end{cases} \quad \text{as} \quad t \to t_s, \tag{77}$$

$$u_{j3} = A_{j3}(t - t_{sd}) + O((t - t_{sd})^2)$$

$$\text{as} \quad t \to t_{sd} \quad \text{for} \quad \frac{r}{\rho} > \frac{c_s}{c_d}, \qquad (78)$$

$$u_{j3} = A_{j3}' \log\left(\left|\frac{t}{t_s} - 1\right|\right) + O(1)$$

$$\text{as} \quad t \to t_s \quad \text{for} \quad \frac{r}{\rho} > \frac{c_s}{c_d}, \qquad (79)$$

for $j = x, y, z$, where the wave-front coefficients are given in the Appendix. These expansions are valid for $0 \leq \theta \leq \pi$, $z > 0$, and $0 \leq c < \infty$, except that (76) is not valid along the rays $x/\rho = c_d/c$ since $A_{j1}$ is unbounded along these rays. Similarly, (77) and (79) are not valid along $x/\rho = c_s/c$, and (78) is not valid along $x/r = c_d/c$.

As the expansions in (76)–(78) show, $u_j$ has a step discontinuity across the hemispherical wave fronts at $t = t_d$ and $t = t_s$, and it is continuous through $t = t_{sd}$. However, for $r/\rho > c_s/c_d$ the disturbance near $t = t_s$ is dominated by the logarithmic singularity shown in (79). This singularity is two-sided in that $u_j$ becomes unbounded as $t \to t_s$ for $t < t_s$ and for $t > t_s$, and it is symmetric about $t = t_s$.

Since the waves trailing behind the load are in an algebraic form, they are expanded algebraically near their wave fronts, yielding

$$u_{j4} = A_{j4}(t - t_{dc})^{-1/2} + O((t - t_{dc})^{1/2}) \quad \text{as} \quad t \to t_{dc}, \qquad (80)$$

$$u_{j5} = \begin{cases} A_{j5}(t - t_{sc})^{-1/2} + O((t - t_{sc})^{1/2}) & \text{for} \quad \dfrac{y}{n} < \phi_c \\ A_{j5}'(t - t_{sc})^{-1/2} + O(1) & \text{for} \quad \dfrac{y}{n} > \phi_c \end{cases}$$

$$\text{as} \quad t \to t_{sc}, \qquad (81)$$

$$u_{j6} = A_{j6}(t - t_{sdc})^{1/2} + O((t - t_{sdc})^{3/2})$$

$$\text{as} \quad t \to t_{sdc} \quad \text{for} \quad \frac{y}{n} > \phi_c, \qquad (82)$$

$$u_{j6} = A_{j6}'(t_{sc} - t)^{-1/2} + O(1) \quad \text{as} \quad t \to t_{sc} \quad \text{for} \quad \frac{y}{n} > \phi_c, \qquad (83)$$

for $j = x, y, z$. These expansions are valid for $0 \leq \theta \leq \pi$ and $z > 0$, except that (80) only arises for $c > c_d$ and $x/\rho \geq c_d/c$, the upper one in (81) for $c > c_d$ and $x/\rho \geq c_s/c$, the lower one in (81) and (83) for $c > c_s$ and $x/\rho \geq c_s/c$, and (82) for $c > c_d$ and $x/r \geq c_d/c$. These latter conditions correspond to when and where the wave fronts $t = t_{dc}$, $t = t_{sc}$, and $t = t_{sdc}$ arise in the half space.

As (80) and (81) show, $u_j$ has a half-order singularity behind the conical wave fronts at $t = t_{dc}$ and $t = t_{sc}$. In addition, $u_j$ contains a half-order singularity in front of $t = t_{sc}$, as (83) shows, producing another two-sided singularity in $u_j$. If $c > c_d$, this two-sided singularity exists across $t = t_{sc}$ for $y/n > \phi_c$; if $c_s < c < c_d$, it exists across the entire conical wave front at $t = t_{sc}$; and if $c < c_s$, it does not exist at all. Also, $u_j$ is continuous through the head wave front at $t = t_{sdc}$, as it is through $t = t_{sd}$. Finally, it should be noted that the disturbance near the wave fronts trailing behind the load is a half-order stronger than near the corresponding wave fronts emanating from the initial position of the load. This can be seen, for example, by comparing the wave-front exsions of $u_{j1}$ as $t \to t_d$ and $u_{j4}$ as $t \to t_{dc}$.

## 6 Stationary Point Load

A special case of the moving load problem is that of a half space whose surface is excited by a stationary point load with step time-dependence. A solution to this problem, which was first worked on by Lamb [15], is obtained here by letting $c \to 0$ in (64)–(70) and expressing the displacements in their cylindrical components, to give

$$u_\sigma(\mathbf{x}, t) = \sum_{\beta=1}^{3} u_{\sigma\beta}(\mathbf{x}, t), \qquad (\sigma = r, z), \qquad (84)$$

$$u_\theta(\mathbf{x}, t) = 0, \qquad (85)$$

for $0 \leq r < \infty$, $0 \leq \theta \leq \pi$, and $0 < z < \infty$, where

$$u_{\sigma 1}(\mathbf{x}, t) = \mathrm{H}(t - t_d) \int_0^{T_d} \mathrm{Re}\left[K_{\sigma d}{}^0(q_d, w) \frac{dq_d}{dt}\right] dw, \qquad (86)$$

$$u_{\sigma 2}(\mathbf{x}, t) = \mathrm{H}(t - t_s) \int_0^{T_s} \mathrm{Re}\left[K_{\sigma s}{}^0(q_s, w) \frac{dq_s}{dt}\right] dw, \qquad (87)$$

$$u_{\sigma 3}(\mathbf{x}, t) = \mathrm{H}(t - t_{sd})\mathrm{H}(t_B - t)\mathrm{H}\left(\frac{r}{\rho} - \frac{c_s}{c_d}\right) \times \int_{A_{sd}}^{T_{sd}} \mathrm{Re}\left[K_{\sigma s}{}^0(q_{sd}, w) \frac{dq_{sd}}{dt}\right] dw, \qquad (88)$$

in which

$$\begin{aligned} K_{rd}{}^0(q, w) &= -iqm_0M, & K_{rs}{}^0(q, w) &= 2iqm_dm_sM \\ K_{zd}{}^0(q, w) &= m_dm_0M, & K_{zs}{}^0(q, w) &= -2m_d(q^2 + w^2)M, \end{aligned} \qquad (89)$$

$$M = \frac{1}{\pi^2 c_d \mu \mathrm{R}}. \qquad (90)$$

The wave geometry associated with these displacements is the same as for $c < c_s$, as shown in Figs. 6(*b*) and 8(*b*), except that the contours $t = t_L$ and $t = t_{sdc}{}^0$ are not present in the $c = 0$ solution.

It should be noted that Eason [16] and Cinelli and Fugelso [17] have also worked on Lamb's point load problem for the interior of the half space using transforms. Their results are also in the form of single integrals, but they do not readily display the wave fronts associated with a concentrated surface load. Mitra [12] has derived the interior displacements for a half space whose surface is excited by a uniform disk of pressure. He also used Cagniard's technique and deHoop's transformation, but in a manner which is somewhat different than here. Furthermore, he mentions that his solution technique is applicable to Lamb's point load problem, but he gives no results. Pekeris [18] has thoroughly analyzed the surface displacements due to a stationary point load. His results agree in detail with those given here if the latter are extended to include $z = 0$. Finally, Lang [19, 20] and Craggs [21] have also worked on Lamb's problem, but they did not use transforms.

Wave-front expansions which correspond to a stationary point load can be computed from the integrals in (86)–(88), or they can be obtained from the expansions in section 5. In fact, these expansions have the same form as those given for $u_{j1}$, $u_{j2}$, and $u_{j3}$ in (76)–(79); the only difference is that the coefficients $A_{j1}$, $A_{j2}$, $A_{j2}'$, $A_{j3}$, and $A_{j3}'$ must be evaluated for $c = 0$. The wave-front expansions for a stationary point load were also computed by Knopoff and Gilbert [22]. They used a Tauberian theorem and the saddle-point technique to evaluate a formal transform solution near the wave fronts. Their results agree in detail with those that are obtained here, except that they did not detect the logarithmic singularity at $t = t_s$ for $r/\rho > c_s/c_d$, as first noted by Aggarwal and Ablow [23].

## 7 Steady-State Response

By algebraic manipulations it can be shown that $u_{j4}$, $u_{j5}$, and $u_{j6}$ in (68)–(70), less $\mathrm{H}(x)$ and $\mathrm{H}(t - t_L)$, are only functions of the coordinates $\xi$, $y$, $z$ which are invariant to the translation of the load (see [14] for details). Therefore, these terms are constant at a fixed position in a coordinate system moving with the load. For $c > c_d$ and long time ($t \to \infty$), $\mathrm{H}(t - t_L) = 1$ and $\mathrm{H}(x) = 1$ for points near the load, and the load "runs away" from the waves emanating from the initial position of the load. Consequently, for $c > c_d$ the waves trailing behind the load represent the steady-state displacement field (i.e., $u_j = u_{j4} + u_{j5} + u_{j6}$ as $t \to \infty$ for $c > c_d$ and points near the position of the load, $j = x, y, z$). The wave geometry corresponding to these steady-state displacements is shown in Fig. 9, where only the waves that trail behind the load are shown.

Lansing [2] has also computed the steady-state displacements due to a moving point load. He used a technique which assumed steady stateness from the outset and his results are in the form of single integrals. As a special case, in the plane under the path of the load ($y$ = 0-plane), and for $\lambda = \mu$ and $c > c_d$, Lansing integrated his results, leaving the displacements in an algebraic form which agrees with that one obtained here.

Finally, for $c < c_d$ the waves trailing behind the load do not represent the entire steady-state displacement field. In this case the waves emanating from the initial position of the load also contribute and they must be evaluated for $t \rightarrow \infty$.

## References


1 Payton, R. G., "An Application of the Dynamic Betti-Rayleigh Reciprocal Theorem to Moving-Point Loads in Elastic Media," *Quarterly of Applied Mathematics*, Vol. 21, 1964, pp. 299–313.

2 Lansing, D. L., "The Displacements in an Elastic Half Space Due to a Moving Concentrated Normal Load," NASA Technical Report, NASA TR R-238, 1966.

3 Mandel, J., and Avramesco, A., "Déplacements Produits par une Charge Mobile à la Surface d'un Semi-Espace Elastique," *Comptes Rendus Des Seánces De L'Academie Des Sciences*, Paris, Vol. 252, Pt. 3, 1961, pp. 3730–3735.

4 Papadopoulos, M., "The Use of Singular Integrals in Wave Propagation Problems, With Application to the Point Source in a Semi-Infinite Elastic Medium," *Proceedings of the Royal Society of London*, Series A, Vol. 276, 1963, pp. 204–237.

5 Papadopoulos, M., "The Elastodynamics of Moving Loads," *Journal of the Australian Mathematical Society*, Vol. 3, 1963, pp. 79–92.

6 Grimes, C. K., "Studies on the Propagation of Elastic Waves in Solid Media," PhD thesis, California Institute of Technology, Pasadena, Calif., 1964.

7 Eason, G., "The Stresses Produced in a Semi-Infinite Solid by a Moving Surface Force," *International Journal of Engineering Science*, Vol. 2, 1965, pp. 581–609.

8 Chao, C. C., "Dynamic Response of an Elastic Half Space to Tangential Surface Loadings," Journal of Applied Mechanics, Vol. 27, No. 3, Trans. ASME, Vol. 82, Series E, Sept. 1960, pp. 559–567.

9 Scott, R. A., and Miklowitz, J., "Transient Non-Axisymmetric Wave Propagation in an Infinite Isotropic Elastic Plate," *International Journal of Solids and Structures*, in press.

10 Cagniard, L., *Reflection and Refraction of Progressive Seismic Waves*, translated by Flinn, E. A., and Dix, C. H., McGraw-Hill, New York, 1962.

11 deHoop, A. T., "A Modification of Cagniard's Method for Solving Seismic Pulse Problems," *Applied Scientific Research*, Section B, Vol. 8, 1959, pp. 349–356.

12 Mitra, M., "Disturbance Produced in an Elastic Half Space by Impulsive Normal Pressure," *Proceedings of the Cambridge Philosophical Society*, Vol. 60, 1964, pp. 683–696.

13 Carslaw, H. S., and Jaeger, J. C., *Operational Methods in Applied Mathematics*, Oxford University Press, 1941.

14 Gakenheimer, D. C., "Transient Excitation of an Elastic Half Space by a Point Load Traveling on the Surface," PhD thesis, California Institute of Technology, Pasadena, Calif., 1969.

15 Lamb, H., "On the Propagation of Tremors Over the Surface of an Elastic Solid," *Philosophical Transactions of the Royal Society of London*, Series A, Vol. 203, 1904, pp. 1–42.

16 Eason, G., "The Displacements Produced in an Elastic Half Space by a Suddenly Applied Surface Force," *Journal of the Institute of Mathematics and Its Applications*, Vol. 2, 1966, pp. 299–326.

17 Cinelli, G., and Fugelso, L. E., "Theoretical Study of Ground Motion Produced by Nuclear Blasts," Mechanics Research Division, American Machine and Foundry Company, report under Contract AF 29(601)-1190 with AFSWC, 1959.

18 Pekeris, C. L., "The Seismic Surface Pulse," *Proceedings of the National Academy of Sciences*, Vol. 41, 1955, pp. 469–480.

19 Lang, H. A., "The Complete Solution for an Elastic Half Space Under a Point Step Load," Report No. P-1141, RAND Corp., Santa Monica, Calif., 1957.

20 Lang, H. A., "Surface Displacements in an Elastic Half Space," *Zeitschrift für angewandte Mathematik und Mechanik*, Vol. 41, 1961, pp. 141–153.

21 Craggs, J. W., "On Axially Symmetric Waves, III. Elastic Waves in a Half Space," *Proceedings of the Cambridge Philosophical Society*, Vol. 59, 1963, pp. 803–809.

22 Knopoff, L., and Gilbert, F., "First Motion Methods in Theoretical Seismology," *Journal of the Acoustic Society of America*, Vol. 31, 1959, pp. 1161–1168.

23 Aggarwal, H. R., and Ablow, C. M., "Solution to a Class of Three-Dimensional Pulse Propagation Problems in an Elastic Half Space," *International Journal of Engineering Science*, Vol. 5, 1967, pp. 663–679.


# APPENDIX

## Wave-Front Coefficients

The wave-front coefficients are written in one expression for all three displacements like the components of a vector.

$$(A_{x1}, A_{y1}, A_{z1}) = (x, y, z)\,\frac{(z/2\pi\mu\rho)a_1}{a_3(a_1^2 + 4r^2za_2)} \tag{91}$$

$$(A_{x2}, A_{y2}, A_{z2}) = (-xz, -yz, r^2)\,\frac{(z/\pi\mu\rho)a_4}{a_6(a_5^2 + 4r^2za_4)} \tag{92}$$

$$(A_{x2}', A_{y2}', A_{z2}') = (-xz, -yz, r^2)\,\frac{(4r^2z^2/\pi\mu\rho)a_7^2}{a_6(a_5^4 + 16r^4z^2a_7^2)} \tag{93}$$

$$(A_{x3}, A_{y3}, A_{z3}) = (xe_1, ye_1, -r)\,\frac{(c_d/\pi\mu r^{3/2})e_1^{3/2}}{e_2^2a_8a_9} \tag{94}$$

$$(A_{x3}', A_{y3}', A_{z3}') = (-xz, -yz, r^2)\,\frac{(z/\pi^2\mu\rho)a_7a_5^2}{a_6(a_5^4 + 16r^4z^2a_7^2)} \tag{95}$$

$$(A_{x4}, A_{y4}, A_{z4}) = (n, yM_d, zM_d)\,\frac{(z/\pi\mu)M_d^{1/2}b_1}{(2cn)^{1/2}(b_1^2 + 4zM_db_2b_3)} \tag{96}$$

$$(A_{x5}, A_{y5}, A_{z5}) = (-nzM_s, -yzM_s^2, b_6)\,\frac{(2z/\pi\mu)M_s^{1/2}b_5}{(2cn)^{1/2}(b_4^2 + 4zM_sb_5b_6)} \tag{97}$$

$$(A_{x5}', A_{y5}', A_{z5}') = (-nzM_s, -yzM_s^2, b_6)\,\frac{(8z^2/\pi\mu)M_s^{3/2}b_6b_7^2}{(2cn)^{1/2}(b_4^4 + 16z^2M_s^2b_6^2b_7^2)} \tag{98}$$

$$(A_{x6}, A_{y6}, A_{z6}) = (\gamma e_1, \gamma e_1M_d, -1)\,\frac{2(2c_d)^{1/2}e_1^{3/2}M_d}{\pi\mu e_2^2b_8^3} \tag{99}$$

$$(A_{x6}', A_{y6}', A_{z6}') = (nzM_s, yzM_s^2, -b_6)\,\frac{(2z/\pi\mu)M_s^{1/2}b_4^2b_7}{(2cn)^{1/2}(b_4^4 + 16z^2M_s^2b_6^2b_7^2)} \tag{100}$$

in which

$$a_1 = (l^2\rho^2 - 2r^2), \qquad a_5 = (\rho^2 - 2r^2)$$
$$a_2 = (l^2\rho^2 - r^2)^{1/2}, \qquad a_6 = \left(1 - \frac{cx}{c_s\rho}\right)$$
$$a_3 = \left(1 - \frac{cx}{c_d\rho}\right), \qquad a_7 = (r^2 - l^{-2}\rho^2)^{1/2} \tag{101}$$
$$a_4 = (l^{-2}\rho^2 - r^2)^{1/2}, \qquad a_8 = (re_1 - z)^{1/2}$$
$$a_9 = \left(1 - \frac{cx}{c_dr}\right)$$

$$b_1 = [n^2(M_s^2 - 1) - 2y^2M_d^2], \qquad b_5 = (z^2M_s^2 - n^2M_{sd}^2)^{1/2}$$
$$b_2 = (z^2M_d^2 + n^2M_{sd}^2)^{1/2}, \qquad b_6 = (y^2M_s^2 + n^2)$$
$$b_3 = (y^2M_d^2 + n^2), \qquad b_7 = (n^2M_{sd}^2 - z^2M_s^2)^{1/2} \tag{102}$$
$$b_4 = [n^2(M_s^2 - 1) - 2y^2M_s^2], \qquad b_8 = (yM_{sd} - zM_d)^{1/2}$$

$$e_1 = (l^2 - 1)^{1/2}, \qquad e_2 = (l^2 - 2) \tag{103}$$

$$M_d = \left(\frac{c^2}{c_d^2} - 1\right)^{1/2}, \qquad M_s = \left(\frac{c^2}{c_s^2} - 1\right)^{1/2},$$
$$M_{sd} = \left(\frac{c^2}{c_s^2} - \frac{c^2}{c_d^2}\right)^{1/2} \tag{104}$$